DEBRIS-LASER BEAM PROBABILITY OF INTERSECTION IN THE PRESENCE OF UNCERTAINTY

Michael Mercurio[(1)], W. R. Faber[(1)], Islam I. Hussein[(1)], Matthew P. Wilkins[(1)], Christopher W. T. Roscoe[(1)], and Paul W. Schumacher, Jr.[(2)]

[(1)]Applied Defense Solutions, Inc., 10440 Little Patuxent Parkway, Suite 600, Columbia, Maryland 21044.
[(2)]Air Force Research Laboratory, 550 Lipoa Parkway, Kihei, Hawaii 96753.

ABSTRACT

Lasers have recently been proposed to "sweep" space debris out of the path of satellites to avoid collision. One of the challenges facing such a technology is the presence of uncertainty in the location of the debris object. Given some uncertainty representation of the debris object state, the probability that the laser beam intersects with a space debris object can be computed. In accordance with recent literature for laser ablation methods, the beam intensity is represented by a Gaussian distribution in the lateral direction, exponentially decaying in the line of sight direction. Further, a particle cloud is used to represent the uncertainty in the debris object state. The probability of intersection between the debris object and the laser beam is then defined and computed. Finally, a probabilistic analysis of the effects of laser ablation on the orbit of debris objects is presented.

1. INTRODUCTION

As the number debris objects in space increases it becomes increasingly difficult to protect assets and operations in space. In recent history, the ability to move or remove debris objects from the operational environment has been a topic of great interest and many different debris removal methods have been proposed. One method in particular is debris removal by ground based laser. When used in conjunction with acquisition and tracking, ground-based lasers can be used to change the orbit of debris objects. Pulsed-laser ablation differs from radiation pressure in that a small portion of the debris object is vaporized, resulting in an impulse to change the current velocity [PAF+96, WZW16]. This procedure can be used to modify the orbit of a debris object, including de-orbiting debris in the LEO regime [PAF+96, MSML11]. Current methods assume the orbit of the debris object is known exactly, and that the intensity profile is constant [Phi14, WZW16, WGJH13]. Mason et. al. provide an expression for constant force on a deterministic debris object from a Gaussian beam with variable intensity, though this method assumes radiation pressure as the momentum transfer mechanism [MSML11]. While approximate expressions for the intensity are applicable for the deterministic case, one must account for the distribution of intensity for a random debris object, as the true state is unknown.

In this paper, we consider the effects of the uncertainty in debris object state on the application of laser-debris removal. We use a particle cloud representation to accurately represent the debris object PDF and its dynamics. This allows us to relax any Gaussian assumptions which are typically assumed in order to approximate the debris object PDF using its first two moments. The laser beam intensity is modeled by a Gaussian distribution to accurately represent the true physical behavior of the beam. Using a Gaussian laser model we determine the beamwidth at range using the principles of laser beam diffraction in order to accurately represent the intersection of a laser and a debris object in a probabilistic fashion.

The remainder of this paper is structured as follows. In section two, we define the debris object representation, the probability of intersection, and the laser beam model. Section three illustrates the effects of uncertainty on the probability of intersection. This is demonstrated by using various space debris removal examples which include different orbital regimes and levels of uncertainty. Lastly in section four, we summarize the contributions of this paper and discuss future work.

2. PROBABILITY OF INTERSECTION

In this section we describe how debris object uncertainty is represented in order to estimate probability of intersection with the laser beam. The debris object uncertainty is modeled using a particle ensemble representation and formulation for the probability of intersection is developed using a Monte Carlo integration.

DISTRIBUTION STATEMENT A. Approved for public release. Distribution is unlimited.

Proc. 7th European Conference on Space Debris, Darmstadt, Germany, 18–21 April 2017, published by the ESA Space Debris Office
Ed. T. Flohrer & F. Schmitz, (http://spacedebris2017.sdo.esoc.esa.int, June 2017)

2.1. Debris Object Uncertainty Representation and Probability of Intersection

Given the probability density function for a space debris object $f(\mathbf{x})$, the probability of intersection, P_I, with a laser beam with a beam coverage volume Ω is defined as

$$P_I = \int_{\Omega} f(\mathbf{x}) \mathrm{d}\mathbf{x}. \tag{1}$$

Even for a Gaussian PDF, $f(\mathbf{x})$ with a compact support volume Ω, the above integral does not have an analytic expression, except for the trivial case when Ω is one-dimensional. Hence, one has to resort to numerical techniques to obtain P_I.

Equation 1 is true only if the beam function is uniform over Ω. However, the beam distribution is not uniform. Let $b(\mathbf{x})$ be the beam distribution function. The probability of intersection in this case is given by:

$$P_I = \int_{\mathbb{R}^3} b(\mathbf{x}) f(\mathbf{x}) \mathrm{d}\mathbf{x}. \tag{2}$$

In this paper we use N_p particles represented by the set of state vectors $\{\mathbf{X}_j\}$, where $j = 1, 2, ..., m$, to describe debris object uncertainty. The particles are initialized by taking N_p samples of the debris object PDF. The particle representation is used to approximate Eq. 2 in the following fashion.

$$P_I = \int b_{\Omega}(\mathbf{x}) f_O(\mathbf{x}) \mathrm{d}\mathbf{x} \simeq \frac{1}{N_p} \sum_{j=1}^{N_p} b(\mathbf{X}_j), \tag{3}$$

where $f_O(\mathbf{x})$ is the debris object PDF represented by the particle ensemble. $b_{\Omega}(\mathbf{x})$ is an indicator function that is equal to 1 if $\mathbf{x} \in \Omega$ and zero otherwise, and where the second integral is over the entire state space. The laser beam model is discussed in the following section.

2.2. Laser Model

In order to accurately determine the probability of intersection, as well as the laser effects on the orbit of the debris object, a beam model must be specified. A simple conic representation similar to that in Figure 1 is not a valid approach, as the governing physics are not well represented, and the beam width is incorrectly computed, e.g. $w(z) \approx 52\ km$ for a range of $z = 1,000\ km$ from some ground station, and a beam divergence (half-angle) of $\theta = 3°$. A beam model is therefore required such that the beam width is determined based on underlying physical processes of the laser.

Ref. [PBL+12] details a beam model which accounts for the beam-width at range via diffraction. Further,

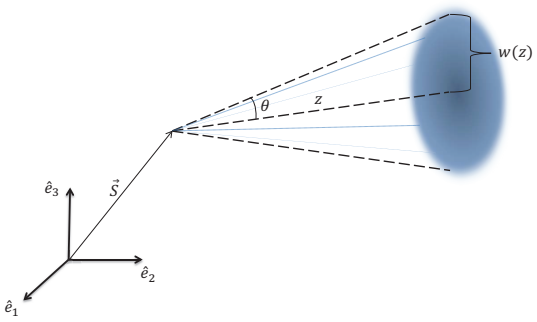

Figure 1. Simple Conic Laser

the model incorporates the "type" of beam chosen (e.g. a Gaussian beam). The corresponding beam width at range z can be expressed as:

$$w(z) = \frac{aM^2 \lambda z}{D_{eff}} \tag{4}$$

where a is the beam-type coefficient, M^2 is the beam quality factor, λ is the laser wavelength, and D_{eff} is the illuminated beam diameter inside the exit aperture (typically expressed as a fraction of the diameter of the focusing optics [MSML11]). The beam width can now be determined for any range z along the beam direction. With this, the specifics of a Gaussian beam can be discussed.

A Gaussian beam implies that both the beam's traverse magnetic and electric field profiles are described by Gaussian density functions. Further, the intensity of the beam is also expressed as a Gaussian density function with variance $w(z)^2$. Thus for a planar section taken at some range z along the beam direction, the intensity profile normal to the beam can be expressed as:

$$I(r|z) = \frac{2W_0}{\pi w(z)^2} \exp\left(\frac{-2r^2}{w(z)^2}\right) \tag{5}$$

where W_0 is the beam power at exit aperture, and r is the radial distance from the beam center. Equation 4 shows that the beam width can be decreased by increasing the effective illuminated diameter. If the debris object were aligned exactly with the beam, a greater intensity could then be delivered. From Eq. 5, the Gaussian intensity profile would possess a lower standard deviation and thus, a more focused region of high intensity. Conversely, if the debris object location is uncertain, a smaller beam width results in a lower probability of intersection.

The Gaussian formulation shows that the intensity delivered to a debris object depends heavily on its

DISTRIBUTION STATEMENT A. Approved for public release. Distribution is unlimited.

position relative to the beam direction. Further, an expression for the illuminated beam area is now available for determination of the probability of intersection with an uncertain orbit. Figure 2 depicts the definition of $3-D$ Intensity Frame for a given realization of the debris object. The beam intensity profile is expressed as a $2-D$ Gaussian distribution in a plane normal to the look direction [MSML11, WGJH13]. The consequences of this formulation on the intersection probability and the laser impingement on a debris object can be discussed.

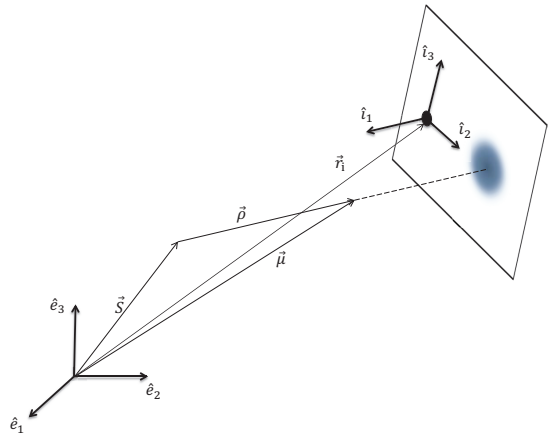

Figure 2. Intensity Frame Definition

3. LASER-DEBRIS REMOVAL APPLICATIONS WITH UNCERTAINTY

This section describes applications of laser beam space debris removal while considering the effects of debris object uncertainty. In particular, viability of the laser-debris removal process will be investigated through a study of the effects of debris object uncertainty initialization on the probability of intersection. Also, laser-debris removal examples are provided to demonstrate laser effects on particle cloud dynamics.

3.1. A Study of the Uncertainty Effects On Probability of Intersection

Both the size of the uncertainty and orientation of the uncertainty with respect to laser will affect the probability of intersection. To give an understanding of the level of tracking accuracy that is required to achieve high levels of P_I, Fig. 3 shows the effect of the size of the uncertainty on the probability of intersection. A debris object was simulated in three different orbital regimes LEO, MEO, and GEO. A Gaussian beam was pointed at the mean location of

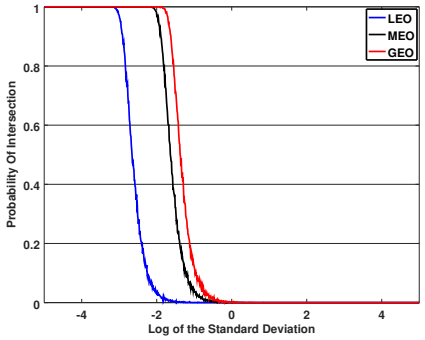

Figure 3. Probability of intersection against the log of the position standard deviation in kilometers

the debris object. The probability of intersection was calculated for a range of uncertainties varying from a position standard deviation of $\sigma_p = 10^{-5}km$ to $\sigma_p = 10^{5}km$. It can be seen that as the uncertainty grows the value of P_I drops rapidly to zero for each orbit regime. This occurs at lower values of standard deviation for the LEO case as opposed to GEO due to the Gaussian beam characteristics and the beam width being dependent on altitude. Further, the rapid decrease in P_I may occur at uncertainty values that are currently unattainable by even the best acquisition and tracking techniques. This asserts that attaining a high value of P_I may not be possible due to the strict limits on the debris object uncertainty.

Aside from the size of the uncertainty, its orientation with respect to the laser also has a significant impact on the P_I. Orientation of the uncertainty is dependent on the type of debris object representation and, if measurement data is being used to update the debris object PDF, the type of measurement data. Figures 4,5 show two hypothetical scenarios in which the P_I is significantly affected by the orientation of the uncertainty. In Fig. 4, the uncertainty is aligned with the line of sight of the laser, which leads to a greater probability of intersection. Figure 5 depicts an orientation that produces lower values of P_I, as many of the debris object realizations are outside of the laser beam.

In Figs. 6,7 a debris object is first simulated in LEO, then MEO, and finally GEO. The simulation is run for a total simulation time of two days using a simulated laser placed in Maui, HI. The probability of intersection is calculated only when the object is in sight of the laser and during the night. The debris objects are represented using a $100,000$ particle ensemble that is initially generated from a Gaussian PDF in Cartesian coordinates. In Fig. 6, the initial standard deviation in position is $\sigma_p = 10^{-3}m$ and in velocity is $\sigma_v = 10^{-4}m/s$. In Fig. 7, the initial standard deviation in position is $\sigma_p = 10^{-1}m$ and in velocity is $\sigma_v = 10^{-2}m/s$.

DISTRIBUTION STATEMENT A. Approved for public release. Distribution is unlimited.

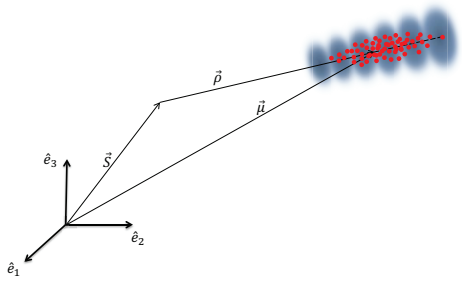

Figure 4. Uncertainty is oriented along the line of sight of the laser.

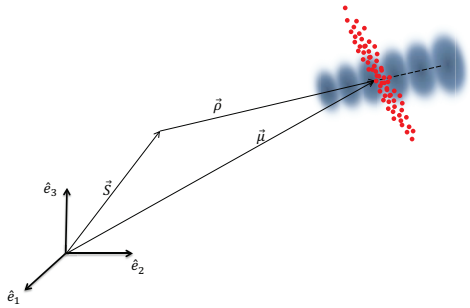

Figure 5. Uncertainty is oriented along the mean velocity vector.

From Figs. 6 and 7, the effect of the age of the data set on the probability of intersection is apparent. It can be seen that as the uncertainty increases, a decrease in probability of intersection is observed. The longer the orbit is propagated without measurement updates, the greater the uncertainty. This suggests that recent and accurate tracking information is required to guarantee laser-debris intersection. Further, it can be seen in Fig. 6 the probability of intersection for the GEO case reaches a value close to one, while the P_I values for the other two cases are lower. This signifies that it is necessary to have more accurate tracking for lower orbital regimes.

The rapid changes depicted in Fig. 7 are likely due to debris object realizations following different orbital trajectories, affecting the number of particles located within the laser beam. Since the laser tracks only the mean of the particle cloud at any given time instant, the uncertainty distribution can affect when/if particles enter the volume of the laser beam. Therefore, particles may enter or exit the volume of the laser beam between time instants, causing oscillations in the value of P_I. These effects are also seen in Fig. 3, although they are not as apparent due to the scale.

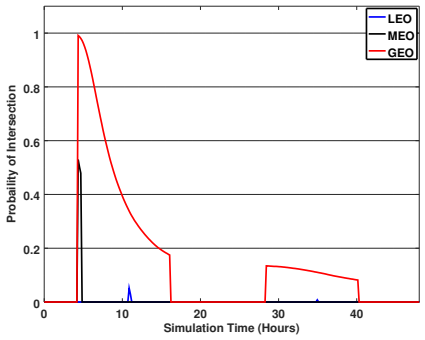

Figure 6. Probability of intersection with debris objects in different orbital regimes. Initial standard deviation set to $\sigma_p = 10^{-3}m, \sigma_v = 10^{-4}m/s$

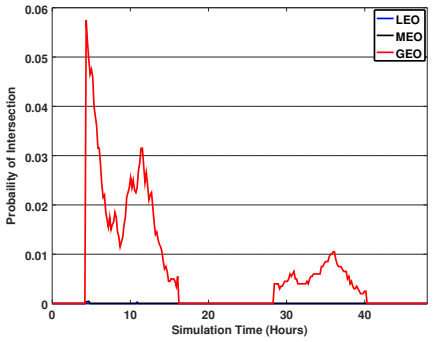

Figure 7. Probability of intersection with debris objects in different orbital regimes. Initial standard deviation set to $\sigma_p = 10^{-1}m, \sigma_v = 10^{-2}m/s$

4. LASER ABLATION FOR ORBIT VARIATION

Extending the application of the previous section, the effects of ground-based lasers on uncertain debris object orbits are discussed. Ground-based lasers can be used to mitigate collision probabilities by maneuvering debris objects away from known assets, or to influence a de-orbiting process [PAF+96, MSML11]. Previously-developed methods assume the orbital state is known exactly, and that the laser is centered on the debris object, allowing for delivery of the maximum possible intensity [LLRP10, MSML11, PAF+96, PBL+12, Phi14, RFT14, WGJH13]. A probabilistic analysis is proposed to account for uncertainty in orbital state and a non-uniform intensity profile on the beam cross section.

The impulsive effect of the laser application can be expressed as a series of discrete Δv events dictated

by the pulse repetition frequency of the laser. The cumulative effect of the laser pulses over some engagement period allows for deviation from an initial orbit. For larger debris objects, multiple engagement periods, or "passes", may be required for an appreciable change in orbit, while a single engagement period may be sufficient for smaller debris objects [MSML11, Phi14].

During the engagement period, the debris object covariance plays a crucial role in the intersection with the laser beam. Too large of a covariance results in a significant reduction in the probability of intersection, limiting the potential applications of the laser. Based upon the analysis of Section 3.1, the analyst should resort to laser ablation if and only if this intersection probability is sufficiently high, e.g. $P_I > 0.9$. For the following examples, it is assumed that this property holds true for the entire engagement period.

For the following analysis, it is assumed the the debris object is spherical in shape, allowing one to neglect attitude properties for all computations. Further, it is also assumed that the laser tracks the mean of the state PDF exactly at all times. The PDF is represented by a particle cloud comprised of N_p equally-weighted particles, where each particle represents a realization of the debris object at any given time. Further, the intensity of the beam assumes a Gaussian distribution at some specified range. These assertions show that a probabilistic investigation is warranted.

From above, the beam width $w(z)$ at a given realization of the debris object is a direct (linear) function of the range z of that realization from the ground station [PAF+96]. This plane is termed the "Intensity Plane" and will be used to investigate the effects of the Gaussian beam on a particle cloud. An approach similar to that developed for conjunction analysis can be carried-out to define the Intensity Plane [Val01].

Figure 8 depicts the Intensity Plane, and the projected realization and beam areas. The position of the realization serves as the origin of the Intensity Frame, and the beam intensity profile is centered at the mean of the state PDF. This clearly demonstrates the effects of orbit state uncertainty and/or laser misalignment on the intensity delivered to the debris object. Several quantities are required in order to determine the effects of the laser on the debris object PDF.

The Intensity Frame is defined via the following unit vectors depicted in Fig. 2:

$$\hat{\mathbf{i}}_1 = -\frac{\boldsymbol{\rho}}{\rho}, \quad \hat{\mathbf{i}}_2 = \hat{\mathbf{i}}_3 \times \hat{\mathbf{i}}_1, \quad \hat{\mathbf{i}}_3 = \frac{\boldsymbol{\rho} \times (\mathbf{r}_i - \mathbf{S})}{||\boldsymbol{\rho} \times (\mathbf{r}_i - \mathbf{S})||} \quad (6)$$

where $\boldsymbol{\rho}$, $\mathbf{S}$, and $\mathbf{r}_i$ are expressed in the ECI frame. From this definition, the Intensity Plane can be formed by sectioning the beam at range z, which is taken to be the altitude of the current realization

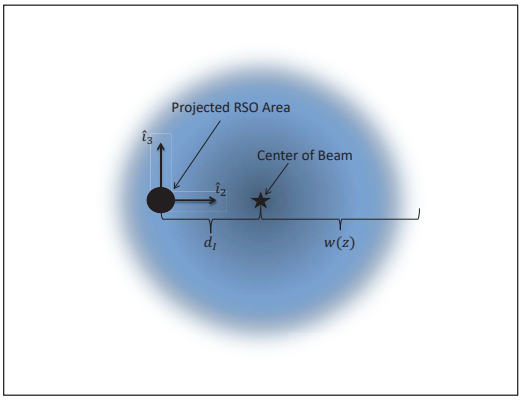

Figure 8. Intensity Plane Schematic

from the ground station along the look direction of the laser, or:

$$z = (\mathbf{r}_i - \mathbf{S}) \cdot \frac{\boldsymbol{\rho}}{\rho} \quad (7)$$

This allows for determination of the Gaussian intensity profile at the correct range for a given realization. The relative distance from the beam center to the debris object is:

$$\mathbf{d} = \mathbf{r}_i - \mathbf{S} - \boldsymbol{\rho} = \mathbf{r}_i - \boldsymbol{\mu} \quad (8)$$

where $\boldsymbol{\mu}$ is the mean of the state PDF. The debris object, the relative distance to the beam center, and the beam itself are then projected onto the Intensity Plane for all subsequent calculations.

Mapping a vector quantity from the ECI frame to the Intensity Frame can be carried-out via a Direction Cosine Matrix (DCM). Since the unit vectors for the Intensity Frame are defined with respect to the ECI frame, the elements of the DCM can be expressed as:

$$\mathbf{C}_{jk} = \hat{\mathbf{i}}_j \cdot \hat{\mathbf{e}}_k, \quad j,k = 1,2,3 \quad (9)$$

The relative distance between the current realization and the center of the Gaussian beam can then be expressed in the Intensity Plane as:

$$\mathbf{d}_I = \begin{bmatrix} 0 & 1 & 0 \\ 0 & 0 & 1 \end{bmatrix} \mathbf{C}\ \mathbf{d} \quad (10)$$

Only the $(\hat{\mathbf{i}}_2, \hat{\mathbf{i}}_3)$ components are retained, as $\hat{\mathbf{i}}_1$ is out-of-plane. With this, the impulsive effects of pulsed-laser ablation can be computed for a given realization.

Ref. [PAF+96] provides a complete overview of momentum coupling theory for pulsed-laser ablation. For brevity, only the main ideas will be presented. Following the definitions above for the Intensity Plane, the Gaussian intensity profile at range z

is expressed in Cartesian space as:

$$I(i_2, i_3|z) = \frac{2W_0}{\pi w(z)^2} \exp\left\{\frac{-2}{w(z)^2}\left[(i_2 - d_I)^2 + {i_3}^2\right]\right\} \tag{11}$$

where (i_2, i_3) are coordinate pairs in the Intensity Plane, and d_I is the magnitude of the relative distance vector $\mathbf{d}_I$. The definitions of the unit vectors specify that the projection of the debris object is colinear with the beam center and thus, the beam center is displaced only horizontally from the origin, i.e. $\mathbf{d}_I \cdot \hat{\mathbf{i}}_2 = d_I$ and $\mathbf{d}_I \cdot \hat{\mathbf{i}}_3 = 0$ (see Figure 8).

For a spherical debris object of radius R, the power delivered to the cross sectional area can be computed as [MSML11, Val01]:

$$W = \int_{-R}^{R} \int_{-\sqrt{R^2 - i_2^2}}^{\sqrt{R^2 - i_2^2}} I(i_2, i_3|z)\ di_3 di_2 \tag{12}$$

The integral over i_3 can be expanded in terms of Error Functions to obtain:

$$W = \sqrt{\frac{2}{\pi}} \frac{W_0}{w(z)^2} \int_{-R}^{R} \left\{ w(z) \exp\left[\frac{-2}{w(z)^2}(i_2 - d_I)\right] \times erf\left(\frac{\sqrt{2}}{w(z)}\sqrt{R^2 - i_2^2}\right)\right\} di_2 \tag{13}$$

The power delivered can be used to determine the magnitude of the impulse applied. For a pulsed laser, the power is delivered instantaneously at discrete times specified by the frequency f of the laser. The fluence (energy per unit area) on the debris object per pulse is expressed as [PAF+96]:

$$\phi = \frac{4WD_{eff}^2}{\pi M^2 a^2 \lambda^2 z^2 f} \tag{14}$$

From momentum coupling theory, the corresponding Δv magnitude can be computed as [PAF+96]:

$$\Delta v = C_m \phi AMR \tag{15}$$

where C_m is the momentum coupling coefficient, and AMR is the area-to-mass ratio for the debris object. The direction of the applied impulse is taken to be the look direction, or:

$$\Delta \mathbf{v} = \Delta v \frac{\boldsymbol{\rho}}{\rho} \tag{16}$$

The development is applied to several test scenarios to investigate the effectiveness of the laser application per orbital regime (LEO, MEO, and GEO). The ground station is known for all cases, and the cumulative effects of the pulsed-laser ablation are examined for a single engagement period of five minutes. The engagement period, and tracking, begins when the mean of the PDF enters the field of regard (FOR) of the ground station. Uncertainty in the debris object is propagated over the engagement period, with no measurement updates performed. The remaining properties of the laser and the debris object are described in Table 1 and Table 2, respectively. Finally, all simulations are carried out by examining the effects of the laser ablation on each realization from the particle cloud.

Property	Value
a	$4/\pi$
M^2	2.0
$\lambda\ (m)$	1.06×10^{-6}
$f\ (Hz)$	1
$W_0\ (W)$	$10,000$
$D_{eff}\ (m)$	2

Table 1. Laser Properties

Property	Value
$R\ (m)$	2.185
$m\ (kg)$	603.3
$AMR\ (m^2/kg)$	0.0249
$C_m\ (N/W)$	75×10^{-6}

Table 2. Debris Object Properties

4.1. Example: LEO Debris Object

This section details the affects of laser ablation on a LEO debris object. The initial time is taken to be the time at which the debris object enters the FOR of the ground station. The statistics of the PDF at this time are assumed Gaussian with (in km and km/s):

$$\boldsymbol{\mu} = [-5,937.3687; 973.36239; 5,311.7010; -4.8949057; -0.86387783; -4.7142366] \tag{17}$$

$$\sigma_p^2 = 1 \times 10^{-4}\ km^2,\ \sigma_v^2 = 1 \times 10^{-6}\ (km/s)^2 \tag{18}$$

The particle cloud is created using $N_p = 2,000$ samples, and the engagement period is assumed to begin at the specified initial time.

Figure 9 depicts the mean of the cumulative Δv applied over the engagement period. It can be seen that the rate at which Δv impulses are added decreases significantly over time. After $t \approx 100\ sec.$, the particle cloud is, on average, receiving very little intensity from the laser beam. This is a result of the small beam width in the LEO regime in concert with the rapidly growing covariance of the debris object. This increases the "spread" of the particle cloud, effectively reducing the number of particles receiving appreciable intensity from the beam. This result shows the effect of the age of the statistical information of the debris object. The less confidence

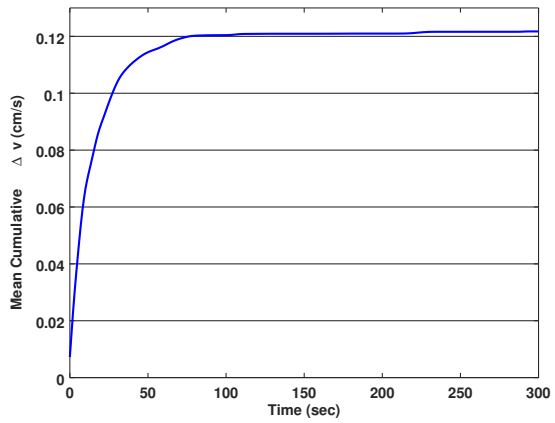

Figure 9. Mean Cumulative Δv - LEO

one has in the debris object position, the less influence the laser will have on the orbit.

Figure 10 depicts a histogram for various cumulative Δv levels experienced by the particle cloud. It can be seen that the majority of realizations receive less than 0.5 cm/s cumulative Δv. Further, approximately 48% of the total number of realizations receive a cumulative Δv less than 1×10^{-9} cm/s, showing that the uncertainty in the debris object position can significantly affect the success of the laser ablation process.

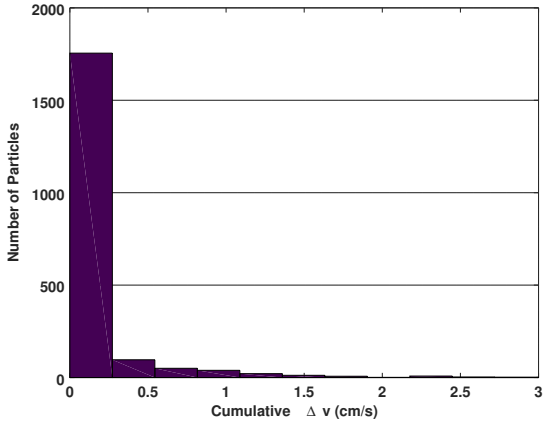

Figure 10. Cumulative Δv Histogram - LEO

Figure 11 depicts the mean change in perigee of the affected particle cloud from the original particle cloud over the engagement period. It can be seen that over the five minute window, the perigee decreases, then begins to increase slowly. This is due to the varying direction of the applied impulse with respect to the mean orbital position of the debris object. Further, the rate at which the perigee is changing decreases over the engagement period. This is a result of the decreasing rate at which Δv impulses are added to the debris object, as shown in Figure 9. Depending on the desired results from the laser ablation (e.g. asset avoidance, de-orbiting, etc.), the engagement period may be adjusted. However, multiple passes may be required for appreciable orbit change due to the low AMR value. Further, orbital influences such as atmospheric drag allow for these deviations to grow over time.

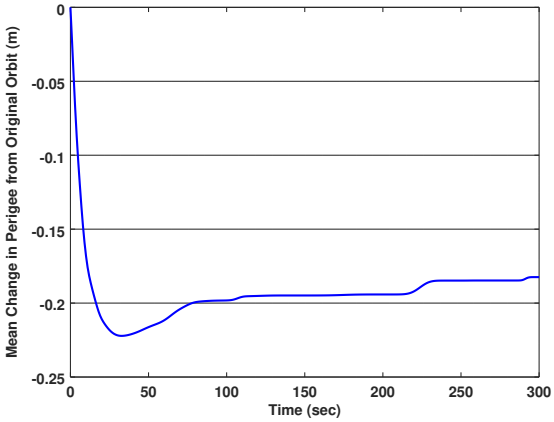

Figure 11. Mean Change in Perigee from Original Orbit - LEO

4.2. Example: MEO Debris Object

This section details the affects of laser ablation on a MEO debris object. The initial time is taken to be the time at which the debris object enters the FOR of the ground station. The statistics of the debris object PDF at this time are assumed Gaussian with (in km and km/s):

$$\boldsymbol{\mu} = [-16,986.411; -10,681.527; 15,7449.308; 2.8885448; -0.78194824; 2.5834162] \quad (19)$$

$$\sigma_p^2 = 1 \times 10^{-4}\ km^2,\ \sigma_v^2 = 1 \times 10^{-6}\ (km/s)^2 \quad (20)$$

The particle cloud is created using $N_p = 2,000$ samples, and the engagement period is assumed to begin at the specified initial time.

Figure 12 depicts the mean of the cumulative Δv applied over the engagement period. It can be seen that, on average, the laser is in contact with the debris object for the entire engagement period. As the debris object moves through the FOV, the range from the ground station increases, effectively reducing the average intensity delivered. Decreases of the rate at which Δv impulses are added are observed. This results in a more gradual slope of the cumulative Δv-t line. While Δv impulses are added throughout the engagement period, their cumulative effect is reduced when compared to that of the LEO case, again illustrating the effects of the orbital regime change.

DISTRIBUTION STATEMENT A. Approved for public release. Distribution is unlimited.

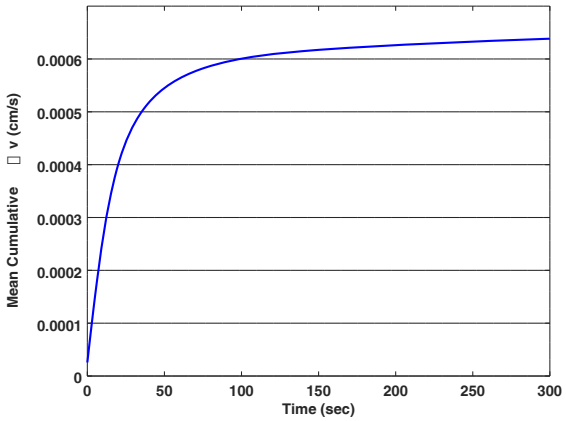

Figure 12. Mean Cumulative Δv - MEO

Figure 13 depicts a histogram of the cumulative Δv values experienced by the particle cloud. It can be seen that, similar to the LEO case, the majority of the particles experience very little cumulative Δv over the engagement period. Unlike the LEO case, the histogram shows a greater range of particles receiving larger cumulative Δv values. This can be attributed to the larger beam width at the MEO altitude, and the low level of uncertainty in the debris object position, allowing for additional particles to receive intensity from the laser. This again demonstrates the combined effect of uncertainty in the debris object, and the increasing beam width on the laser application.

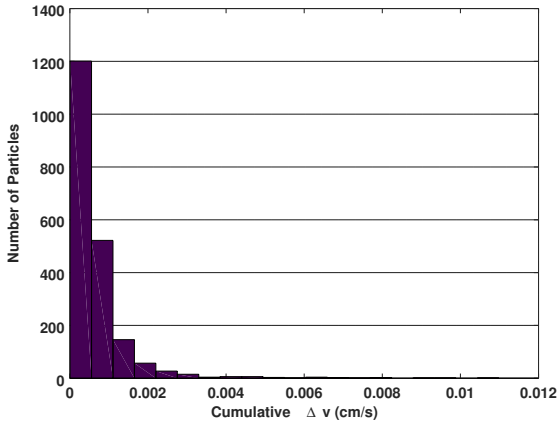

Figure 13. Cumulative Δv Histogram - MEO

Figure 14 depicts the mean variation in perigee of the laser-affected particle cloud from the original particle cloud. By the end of the engagement period, the maximum change in perigee is approximately 0.0325 m. In comparison to the LEO case, this is a reduction of approximately one order of magnitude for the same engagement period. This shows the effect of the orbital regime on the available laser applications. Further, as opposed to the LEO case, the perigee increases for the duration of the engagement, as the Δv impulses decrease the orbital kinetic energy. Additionally, the lower kinetic energy in the MEO regime implies that throughout the short engagement window, the direction of the applied Δv impulses does not vary appreciably. Finally, the continued variation in perigee is due to the larger beam width in the MEO regime, allowing for a larger number of particles to receive intensity from the laser.

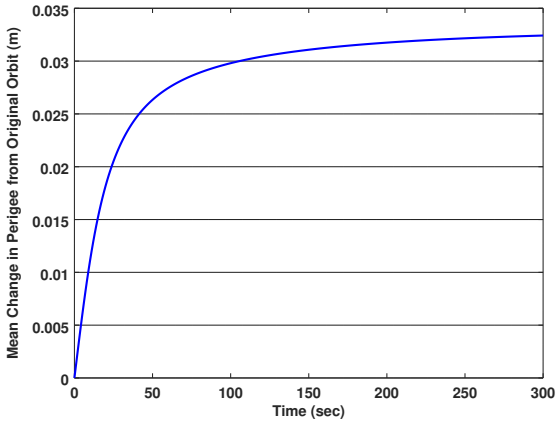

Figure 14. Mean Change in Perigee from Original Orbit - MEO

4.3. Example: GEO Debris Object

For a final investigation, the effects of laser influence on a GEO debris object are considered. The statistics of the PDF at the initial engagement time are assumed Gaussian with (in km and km/s):

$$\boldsymbol{\mu} = [\,-31,506.337; 27,860.124; 3,654.1208; \\ -2.0275442; -2.201101; -0.70126677] \quad (21)$$

$$\sigma_p^2 = 1 \times 10^{-4}\ km^2,\ \sigma_v^2 = 1 \times 10^{-6}\ (km/s)^2 \quad (22)$$

The particle cloud is created using $N_p = 2,000$ samples, and the engagement period is assumed to begin at the specified initial time.

Figure 15 depicts the mean cumulative Δv applied over the engagement period. A similar trend to the MEO case is seen, where, on average, the debris object is always within the FOR, but the increasing range from the ground station affects the magnitudes of the applied Δv impulses towards the end of the engagement period. Further, the mean of total applied Δv is on the same order of magnitude as that of the MEO case.

Finally, Figure 16 depicts the cumulative Δv histogram. Of the three cases examined, the GEO

DISTRIBUTION STATEMENT A. Approved for public release. Distribution is unlimited.

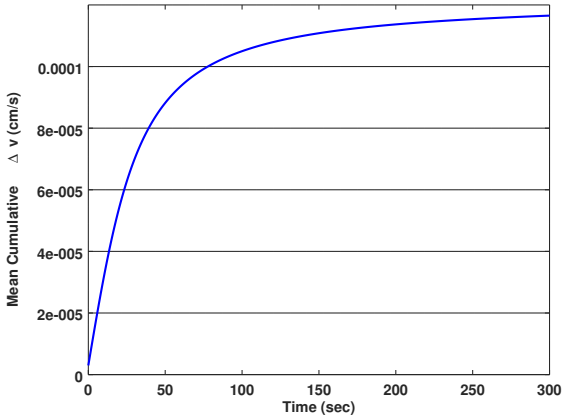

Figure 15. Mean Cumulative Δv - GEO

case exhibits the greatest range of particles attaining greater-than-zero cumulative Δv levels. Similar to the MEO case, this is due to the larger beam width at GEO, coupled with the low level of uncertainty in the debris object location. These two points allow for additional particles to receive impulsive influence from the laser.

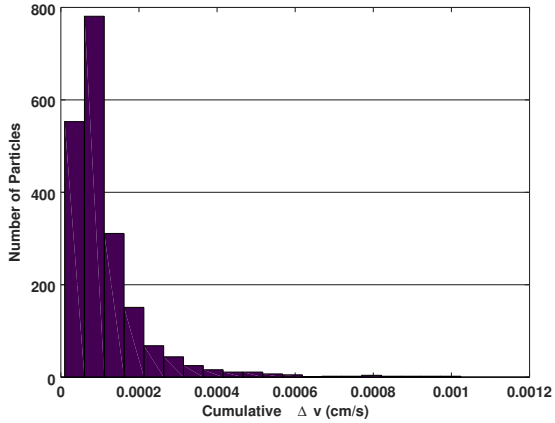

Figure 16. Cumulative Δv Histogram - GEO

Figure 17 depicts the mean variation in perigee between the laser-affected particle cloud and the original particle cloud. It can be seen that, as expected, the change in orbital regime adversely affects the maximum change in perigee. Comparing with previous results, the maximum change in the mean perigee is two orders of magnitude less than the LEO case and one order of magnitude less than the MEO case. Again, the effect of the orbital regime on the laser application is apparent. Further, as a result in the increased beam width, and lower orbital kinetic energy, the trend at which the perigee increases is similar to that of the MEO case. The effect of the increased range from MEO to GEO is more apparent in the magnitude of the perigee variation and the cumulative Δv magnitudes.

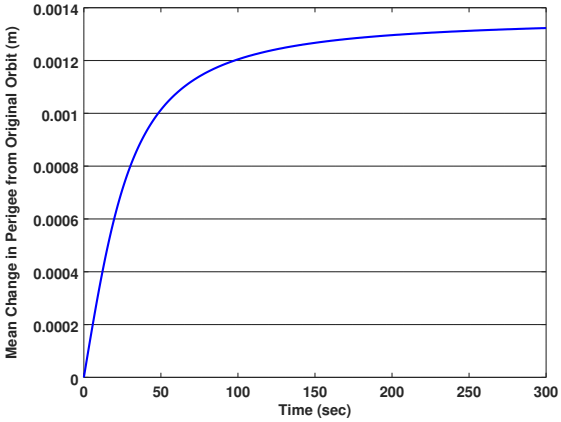

Figure 17. Mean Change in Perigee from Original Orbit - GEO

5. CONCLUSIONS

In this paper, we modeled uncertainty in debris object state and developed techniques to incorporate this uncertainty into laser debris removal analysis. Previous research efforts in laser-influenced debris removal have assumed perfect knowledge of the debris object's orbital state, while this research has shown that the effects of this uncertainty over time cannot be ignored or understated.

Through an investigation on the effects of debris object uncertainty on the probability of intersection, it has been shown that size and orientation are crucial in calculating an accurate value for P_I. This in turn shows that uncertainty effects cannot be ignored in laser debris removal analysis. The level of tracking accuracy required to guarantee intersection depends on the laser characteristics. For lower orbital regimes, the required tracking accuracy is highest.

Investigating the direct effects of laser-influenced debris, it can be seen that the orbital regime plays a significant role in the effects of the laser ablation process. For a given orbital regime, one must choose whether or not to employ the ablation process depending on the desired outcome. For the LEO debris object, the magnitude of the applied Δv is, on average, significantly greater than the MEO and GEO cases, allowing for the most substantial effects. This is expected due to the increase in range from the ground station for each subsequent regime. However for the parameters chosen, the growth in the uncertainty out-paces that of the beam width for the LEO regime, resulting in a significant decrease in the number of particles receiving intensity. Finally, in all cases considered, the majority of the debris ob-

DISTRIBUTION STATEMENT A. Approved for public release. Distribution is unlimited.

ject realizations from the particle cloud receive little intensity from the laser. However, as the orbit altitude increases, the number of debris-object realizations receiving greater Δv values increases due to the increasing beam width. Thus, alongside the beam width at altitude, the orbit uncertainty level plays a crucial role in both the acquisition of the debris, and the likelihood of influencing the orbit via laser ablation.

REFERENCES

LLRP10. Duane A Liedahl, Stephen B Libby, Alexander Rubenchik, and Claude Phipps. Momentum transfer by laser ablation of irregularly shaped space debris. In AIP Conference Proceedings, volume 1278, pages 772–779. AIP, 2010.

MSML11. James Mason, Jan Stupl, William Marshall, and Creon Levit. Orbital debris–debris collision avoidance. Advances in Space Research, 48(10):1643–1655, 2011.

PAF+96. CR Phipps, G Albrecht, H Friedman, D Gavel, EV George, J Murray, C Ho, W Priedhorsky, MM Michaelis, and JP Reilly. Orion: Clearing near-earth space debris using a 20-kw, 530-nm, earth-based, repetitively pulsed laser. Laser and Particle Beams, 14(1):1–44, 1996.

PBL+12. Claude R Phipps, Kevin L Baker, Stephen B Libby, Duane A Liedahl, Scot S Olivier, Lyn D Pleasance, Alexander Rubenchik, James E Trebes, E Victor George, Bogdan Marcovici, et al. Removing orbital debris with lasers. Advances in Space Research, 49(9):1283–1300, 2012.

Phi14. Claude R Phipps. A laser-optical system to re-enter or lower low earth orbit space debris. Acta Astronautica, 93:418–429, 2014.

RFT14. Alexander M Rubenchik, Michail P Fedoruk, and Sergei K Turitsyn. The effect of self-focusing on laser space-debris cleaning. Light: Science & Applications, 3(4):e159, 2014.

Val01. David A Vallado. Fundamentals of astrodynamics and applications, volume 12. Springer Science & Business Media, 2001.

WGJH13. E Wnuk, J Golebiewska, C Jacquelard, and H Haag. Changes of space debris orbits after ldr operation. In Advanced Maui Optical and Space Surveillance Technologies Conference, 2013.

WZW16. Chenglin Wang, Yan Zhang, and Kunpeng Wang. Impulse calculation and characteristic analysis of space debris by pulsed laser ablation. Advances in Space Research, 58(9):1854–1863, 2016.

DISTRIBUTION STATEMENT A. Approved for public release. Distribution is unlimited.